Notes on Numerical Fluid Mechanics
and Multidisciplinary Design 151

Andreas Dillmann
Gerd Heller
Ewald Krämer
Claus Wagner *Editors*

New Results in Numerical and Experimental Fluid Mechanics XIII

Contributions to the 22nd STAB/DGLR Symposium

Springer

Notes on Numerical Fluid Mechanics and Multidisciplinary Design

Volume 151

Notes on Numerical Fluid Mechanics and Multidisciplinary Design publishes state-of-art methods (including high performance methods) for numerical fluid mechanics, numerical simulation and multidisciplinary design optimization. The series includes proceedings of specialized conferences and workshops, as well as relevant project reports and monographs.

More information about this series at http://www.springer.com/series/4629

Andreas Dillmann · Gerd Heller ·
Ewald Krämer · Claus Wagner
Editors

New Results in Numerical and Experimental Fluid Mechanics XIII

Contributions to the 22nd STAB/DGLR Symposium

Springer

Editors
Andreas Dillmann
Deutsches Zentrum für Luft und Raumfahrt,
Institut für Aerodynamik und
Strömungstechnik
Göttingen, Niedersachsen, Germany

Ewald Krämer
Institut für Aerodynamik und Gasdynamik
Universität Stuttgart
Stuttgart, Baden-Württemberg, Germany

Gerd Heller
Airbus Deutschland
Bremen, Bremen, Germany

Claus Wagner
Deutsches Zentrum für Luft und Raumfahrt,
Institut für Aerodynamik und
Strömungstechnik
Göttingen, Niedersachsen, Germany

ISSN 1612-2909 ISSN 1860-0824 (electronic)
Notes on Numerical Fluid Mechanics and Multidisciplinary Design
ISBN 978-3-030-79560-3 ISBN 978-3-030-79561-0 (eBook)
https://doi.org/10.1007/978-3-030-79561-0

This Springer imprint is published by the registered company Springer Nature Switzerland AG
The registered company address is: Gewerbestrasse 11, 6330 Cham, Switzerland

Preface

STAB is the German Aerospace Aerodynamics Association (Deutsche Strömungsmechanische Arbeitsgemeinschaft) founded in the late 1970s, and DGLR is the German Society for Aeronautics and Astronautics (Deutsche Gesellschaft für Luft- und Raumfahrt - Lilienthal Oberth e.V.). The mission of STAB is to foster aerodynamics research and its appreciation in Germany. This is accomplished by creating forums for scientific discussions and by disseminating most recent research results, thereby promoting scientific progress and avoiding unnecessary duplication in research.

STAB brings together German scientists and engineers from universities, research establishments and industry. They present research and project work in numerical and experimental fluid mechanics as well as aerodynamics for a wide variety of fields, such as aeronautics, space, ground transportation, wind turbines and other applications. This format also offers an excellent opportunity for exchange on numerous joint research activities supported by different funding agencies.

Since 1986, the symposium has taken place every two years at different locations in Germany, all having an affinity with fluid mechanics and aerodynamics.

In addition, STAB workshops are regularly held at Deutsches Zentrum für Luft- und Raumfahrt (DLR) in Göttingen in the intermediate years.

Both STAB symposia and workshops provide excellent forums where new research activities can be presented, often resulting in new jointly organized research and technology projects.

In 2020, the 22nd DGLR/STAB Symposium was planned to be held in Berlin. Unfortunately, due to the corona pandemic, the STAB Board had to cancel the conference to protect the health of the participants.

However, it was the Board's strong ambition to give researchers who had planned a presentation for the symposium the opportunity to publish their latest work in an appropriate setting. Thus, the present volume contains the papers originally envisaged for the symposium after having successfully undergone a thorough peer review process.

The review panel for the papers included in this volume consisted of

G. Babij (Göttingen); P. Bahavar (Göttingen); C. Bauer (Göttingen); A. Bauknecht (Braunschweig); P. Bekemeyer (Braunschweig); J. Bell (Göttingen); C. Birkenmaier (Regensburg); K. Bock (Dresden); F. Boden (Göttingen); J. Bosbach (Göttingen); J. Braukmann (Göttingen); C. Breitsamter (München); C. Brückner (Göttingen); M. Cerny (München); M. Cormier (Stuttgart); A. Dannhauer (Göttingen); K. Ehrenfried (Göttingen); M. Ehrle (Stuttgart); S. Fechter (Göttingen); M. Fehrs (Göttingen); J. Feldwisch (Göttingen); U. Fey (Göttingen); J. Franco Sumariva (Göttingen); A. Franco (Braunschweig); M. Franze (Braunschweig); L. Gagnon (Stuttgart); A. Gardner (Göttingen); N. Gauger (Kaiserslautern); F. Genuit (Stuttgart); V. Hannemann (Göttingen); S. Hein (Göttingen); D. Heine (Göttingen); S. Helm (Göttingen); M. Herr (Göttingen); M. Hillebrand (Stuttgart); I. Huismann (Dresden); T. Hüttl (Ismaning); F. Jäckel (Göttingen); S. Jakirlic (Darmstadt); C. Kaiser (Göttingen); M. Keßler (Stuttgart); T. Kirmse (Göttingen); M. Klein (Cottbus); C. Klein (Göttingen); T. Knopp (Göttingen); A. Kohl (Göttingen); N. Krimmelbein (Braunschweig); A. Krumbein (Göttingen); P. Lange (Göttingen); J. Löwe (Göttingen); T. Lutz (Stuttgart); J. Martinez Schramm (Göttingen); E. Mäteling (Aachen); C. Merrem (Braunschweig); O. Meyer (Neubiberg); U. Michel (Berlin); M. Mommert (Göttingen); M. Müller (Göttingen); J. Müller (Stuttgart); K. Niehaus (Göttingen); R. Olmeda (München); R. Pochampalli (Kaiserslautern); A. Probst (Göttingen); D. Puckert (Stuttgart); A. Raichle (Braunschweig); L. Reimer (Braunschweig); M. Rein (Göttingen); C. Reinbold (München); S Risius (Göttingen), U. Rist (Stuttgart); L. Rottmann (Braunschweig); J. Ruhland (München); S. Satcunanathan (Aachen); D. Schiepel (Göttingen); L. Schmidt (Göttingen); M. Schollenberger (Stuttgart); G. Schrauf (Braunschweig); E. Schülein (Göttingen); M. Schulze (Göttingen); D. Schütz (Siegen); A. Shishkin (Göttingen); L. Siegel (Göttingen); D. Simanowitsch (Göttingen); M. Soni (Braunschweig); C. Stemmer (München); L. Streher (Braunschweig); T. Streit (Braunschweig); E. Tangermann (Neubiberg); A. Theiss (Göttingen); G. Voss (Göttingen); A. Waldmann (Stuttgart); V. Wartemann (Braunschweig); K. Weinman (Göttingen); M. Weinschenk (Stuttgart); A. Westhoff (Göttingen); T. Wetzel (Hamburg); H. Wilhelmi (Göttingen); G. Wilke (Braunschweig); C. Wolf (Göttingen); J. Yin (Braunschweig); R. Zahn (München); B. Zhou (Kaiserslautern).

Contents

Airplane Aerodynamics/Propulsion Integration

Influence of the Wind Tunnel Model Mounting on the Wake Evolution of the Common Research Model in Post Stall 3
Maximilian Ehrle, Andreas Waldmann, and Thorsten Lutz

Assessment of the Disturbance Velocity Approach to Determine the Gust Impact on Airfoils in Transonic Flow 14
Jens Müller, Marco Hillebrand, and Thorsten Lutz

Comparison of Different Methods for the Extraction of Airfoil Characteristics of Propeller Blades as Input for Propeller Models in CFD 24
Michael Schollenberger and Thorsten Lutz

Turbulence and Transition

Effect of the Motion Pattern on the Turbulence Generated by an Active Grid 37
Meike Herbert, Tanja Skeledzic, Hermann Lienhart, and Özgür Ertunc

Stochastic Modeling of Passive Scalars in Turbulent Channel Flows: Predictive Capabilities of One-Dimensional Turbulence 47
Marten Klein and Heiko Schmidt

Study of RANS Turbulence Models for Turbulent Wake Flow in Adverse Pressure Gradient 58
Tobias Knopp, Paul Korsmeier, Mikael Strelets, and Ekaterina Guseva

Study on Large-Scale Amplitude Modulation of Near-Wall Small-Scale Structures in Turbulent Wall-Bounded Flows 68
Esther Mäteling, Michael Klaas, and Wolfgang Schröder

Application of Multitask Learning for Enhancement of Spalart-Allmaras Turbulence Model 77
Rohit Pochampalli, Emre Özkaya, Beckett Y. Zhou, Guillermo Suarez, and Nicolas R. Gauger

Investigation of Coherent Motions in a Flat-Plate Turbulent Boundary Layer with Adverse Pressure Gradient 87
Matthias Weinschenk, Ulrich Rist, and Christoph Wenzel

Hypersonic Aerothermodynamics

HyperCODA – Extension of Flow Solver CODA Towards Hypersonic Flows 99
Immo Huismann, Stefan Fechter, and Tobias Leicht

Experimental Approach on Concentration Measurements of NO in Hydrogen Combustion Based on Heterodyne Laser Absorption Spectroscopy Using Quantum Cascade Lasers 110
Jan Martinez Schramm and Diana Luís

Internal Application of Ultra-Fast Temperature Sensitive Paint to Hydrogen Combustion Flow 121
Jan Martinez Schramm and Leni Schmidt

Aerodynamic Data Set Generation for the Experimental Vehicle ReFEx 132
Clemens Merrem, Viola Wartemann, and Thino Eggers

Contribution of Numerical and Experimental Flow Simulations to the Aerodynamic Data Base of the DLR Reusable Flight Experiment ReFEx 141
Viola Wartemann, Ntarinai Konosidou, Andreas Flock, and Clemens Merrem

Flow Control

Unsteady Characterization of Fluidic Flow Control Devices for Gust Load Alleviation 153
Salvatore Asaro, Khalid Khalil, and André Bauknecht

Aeroelastic Behavior of a Laminar Wing in Transonic Flow 164
Michael Fehrs, Sebastian Helm, Christoph Kaiser, and Thomas Klimmek

Influence of Surface Irregularities on the Expected Boundary-Layer Transition Location on Hybrid Laminar Flow Control Wings 174
Juan Alberto Franco Sumariva, Alexander Theiss, and Stefan Hein

Transition Prediction and Analysis of the CRM-NLF Wing with the DLR TAU Code 185
Sebastian Helm, Michael Fehrs, Normann Krimmelbein, and Andreas Krumbein

Determination of Critical N-Factors for the CRM-NLF Wing 195
Normann Krimmelbein and Andreas Krumbein

Experimental Investigation on Roughness-Induced Transition Under the Influence of Freestream Turbulence 205
Dominik K. Puckert, Tristan M. Römer, Giacomo Scibelli, and Ulrich Rist

A Procedure to Estimate the Size of a Suction Flap for a Passive HLFC System 215
Geza Schrauf

Receptivity of Swept-Wing Boundary Layers to Surface Roughness and Inhomogeneous Suction 224
Daniel Simanowitsch, Alexander Theiss, and Stefan Hein

DLR Feasibility Study of HLFC Wing Designs for S1MA Wind Tunnel Test 235
Thomas Streit, Heiko Geyr von Schweppenburg, David Cruz, and Rafael Sanchez

The Effect of 2-D Surface Irregularities on Laminar-Turbulent Transition: A Comparison of Numerical Methodologies 246
Francesco Tocci, Juan Alberto Franco, Stefan Hein, Guillaume Chauvat, and Ardeshir Hanifi

Numerical Study of Dynamic 2D Bumps for Active Gust Load Alleviation 257
Junaid Ullah, Ferdinand Seel, and Thorsten Lutz

High-Agility Configuration

Steady-State Flow Solutions for Delta Wing Configurations at High Angle of Attack Using Implicit Schemes 271
Arpit Aggarwal, Ralf Hartmann, Stefan Langer, and Tobias Leicht

Analysis of Vortex Burst Phenomena on Generic Hybrid Delta Wing Planforms at Subsonic Speeds 282
Dominik Sedlacek, Florian M. Heckmeier, Artur Usbek, and Christian Breitsamter

Numerical Modelling of a Wind Tunnel Experiment to Investigate Vortex-Dominated Flow at Medium and High Angles of Attack 292
Guido Voss

Rotorcraft

Investigation of a Coaxial Propeller Configuration Under Non-axial Inflow Conditions 305
Michael Cerny, Jan-Arun Faust, and Christian Breitsamter

BOS-Based Three-Dimensional Reconstruction of Rotor Blade Tip Vortex Positions 315
Nicola Debernardis, Clemens Schwarz, and Johannes N. Braukmann

Quantification of the Influence of Particle Voids on PIV Measurements via Synthetic-PIV 325
Vincent Domogalla

Development and Analysis of a Coaxial Rotor Test Bench in Axial Flow Conditions 335
Jan-Arun Faust, Nikolai Herzog, Michael Cerny, and Christian Breitsamter

Numerical Investigation of Aerodynamic Fairings on a Cycloidal Rotor 345
Louis Gagnon

Application of Fan Boundary Condition for Modelling Helicopter Rotors in Vertical Flight 355
Anna A. Kostek, Katarzyna Surmacz, Michał Rajek, and Tomasz Goetzendorf-Grabowski

Efficient Aerodynamic and Aeroacustic Optimization of Propeller Sections Using Bayesian Methods 365
Andreas Kümmel and Christian Breitsamter

Approximate Boundary Layer Methods for a Fast Mid-Fidelity Aerodynamics Code for Helicopter Simulations 376
Philipp Kunze

Experimental Measurement of a UAV Rotor's Acoustic Emission 387
Felix Lößle, Anna Kostek, Clemens Schwarz, and Rainer Schmid

Aerodynamic Analysis and Optimization of a Coaxial Helicopter Fuselage 397
Lukas Rottmann

Effect of Vortex-Wake Interaction on Vortex-Rotor Interference and on Rotor Trim 407
Berend G. van der Wall

Comparisons of Different Spatial Schemes and Limiters for Helicopter Flows 418
Gunther Wilke

Experimental and Numerical Study on Helicopter Acoustic Scattering 428
Jianping Yin and Karl-Stéphane Rossignol

Technical Flows

Bi-stability Detection in the Flow Around a Sphere by Means of Experiments and Lattice Boltzmann Simulations 441
Christian Bauer, Max Müller, Klaus Ehrenfried, and Claus Wagner

Convolutional Neural Networks for Approximation of Blood Flow in Artificial Lungs 451
Clemens Birkenmaier and Lars Krenkel

Modelling of Heat Transfer for Droplet Condensation in Mixed Convective Duct Flow 461
Christian Brückner, Andreas Westhoff, and Claus Wagner

Experimental Simulation of the Human Respiration 472
Andreas Kohl, Pascal Lange, and Daniel Schmeling

Characterization of a Mixed Convection Cell Designed for Phase Transition Studies in Moist Air 483
Konstantin A. Niehaus, Andreas Westhoff, and Claus Wagner

Study on the Influence of Turbulence on Thermal Comfort for Draft Air 494
Daniel Schiepel and Andreas Westhoff

On the Simulation of a Heavy Vehicle Wake in OpenFOAM with Real-World Data 504
Keith A. Weinman, Henning Wilhelmi, James R. Bell, Daniela Heine, and Claus Wagner

Aerodynamic Characterisation of a Compact Car Driving Behind a Heavy Vehicle 514
Henning Wilhelmi, Christoph Jessing, James R. Bell, Daniela Heine, Joachim Wiedemann, Andreas Wagner, and Claus Wagner

Aeroelasticity and Structural Dynamics

High-Fidelity Aeroelastic Loads Calculation for a Transport Aircraft Configuration Including Pitch and Roll Maneuvers 527
Johan Moritz Feldwisch and Matthias Schulze

Deformation Measurements of a Full Span Model with Adaptive Elasto-Flexible Membrane Wings 537
Jonathan Pflüger, Yuting Chen, and Christian Breitsamter

Numerical Investigation of Flexibility Effects on the CFD-CSM Coupling of Deflected Delta Wing Control Surfaces 547
Christopher Reinbold, Kaare Sørensen, and Christian Breitsamter

Fluid and Thermodynamics

Validation of a Dynamic Simulation Approach for Transient Performance Using the Example of a Turbojet Engine 559
Jan Göing, Johannes Hogrefe, Sebastian Lück, and Jens Friedrichs

LES of N2/H2 Transcritical Injection in a Rocket Combustion Chamber 569
Raffaele Olmeda and Christian Stemmer

Computational Aerodynamics

Towards a 3D Galerkin-Type High-Order Panel Method: A 2D Prototype 581
Karsten Bock

Numerical Investigation of the Unsteady Flow Field Past an Offshore Wind Turbine in Maintenance Operations 592
Marion Cormier and Thorsten Lutz

A Discontinuous Galerkin Chimera Method for Unsteady Flow Problems on Moving Grids 604
Fabian Genuit, Manuel Keßler, and Ewald Krämer

Efficient Modelling of Near-Wall Turbulence in Hybrid RANS-LES Simulations 615
Marius Herr and Axel Probst

Sensitivity Analysis of Discrepancy Terms Introduced in Turbulence Models Using Field Inversion 625
Florian Jäckel

Spliss: A Sparse Linear System Solver for Transparent Integration of Emerging HPC Technologies into CFD Solvers and Applications . . . 635
Olaf Krzikalla, Arne Rempke, Alexander Bleh, Michael Wagner, and Thomas Gerhold

Convection Treatment for RANS Turbulence Model Equations 646
Sebastian Braun, Stefan Langer, and Tobias Leicht

DES of Weapon Bay in Fighter Aircraft Under High-Subsonic and Supersonic Conditions 656
Karthick Rajkumar, Eike Tangermann, Markus Klein, Sebastian Ketterl, and Andreas Winkler

Numerical Investigation of a Porous Trailing Edge by a Zonal RANS/LES Simulation 666
Sutharsan Satcunanathan, Matthias Meinke, and Wolfgang Schröder

Meshing Strategy for Movable Control Surfaces: Towards High-Fidelity Flight Maneuver Simulations 677
Larissa Bruna Streher and Ralf Heinrich

Aerodynamic Shape Design of a Powered Helicopter Cell Using an Adjoint RANS Method with Actuator Disk Modelling 687
Jan-Hendrik Wendisch, Marc Wentrup, and Arthur Stück

Neural Network Modeling of Transonic Buffet on the NASA Common Research Model 697
Rebecca Zahn, Tim Linke, and Christian Breitsamter

Experimental Aerodynamics

Experimental Investigation of a Line-Cavity System Equipped with Fiber-Optic Differential Pressure Sensors in a Shock Tube 709
Florian M. Heckmeier, Niklas Mooshofer, Thomas Hopfes, Christian Breitsamter, and Nikolaus A. Adams

2D Airfoil-Testing in an Open Wind Tunnel Test Section: Test Setup, Instrumentation, Interference-Corrections, Validation 719
Oliver Meyer

On the Effectiveness of Retrofitted Airfoil Leading Edge Devices to Limit Lift 729
Oliver Meyer

Wake Vortex Analysis on Transport Aircraft Wing Featuring Dynamic Flap Motion 739
Johannes Ruhland and Christian Breitsamter

Aeroacoustic Noise

Fast Non-empiric Propeller Source Noise Model with Mean Flow 751
Andrea Franco, Roland Ewert, Malav Mukesh Soni, Michael Mößner, and Jan Werner Delfs

Investigation of Lighthill-Source Components in a Planar Jet-Wing-Flap Configuration 761
Daniel Schütz and Holger Foysi

A FWH Method for Aeroacoustic Prediction in Presence of Vorticity and Convection 773
Daniel Schütz and Holger Foysi

Author Index 785

Airplane Aerodynamics/Propulsion Integration

Influence of the Wind Tunnel Model Mounting on the Wake Evolution of the Common Research Model in Post Stall

Maximilian Ehrle(✉), Andreas Waldmann, and Thorsten Lutz

Faculty 6: Aerospace Engineering and Geodesy, Institute of Aerodynamics and Gas Dynamics, University of Stuttgart, Stuttgart, Germany
{ehrle,waldmann,lutz}@iag.uni-stuttgart.de

Abstract. This work describes the influence of the wind tunnel support system on the wake flow and associated forces acting on the CRM aircraft configuration in post-stall conditions at subsonic Mach numbers. Unsteady scale-resolving simulations at $\alpha = 18°$, $M_\infty = 0.25$ and $Re_\infty = 11.6 \cdot 10^6$ were carried out using the CRM with and without a support sting, respectively. A predominantly local effect of the sting was observed at these conditions, causing significant deflection of the local flow direction near the sting. The sting's shape causes downward deflection near the horizontal tailplane, decreasing that surface's effective angle of attack and its lift coefficient. This results in a reduced overall lift coefficient C_L and a significantly reduced nose-down pitching moment C_{My}. The wing pressure distribution is only weakly affected.

Keywords: Transport aircraft · Stall · Hybrid RANS/LES methods

1 Introduction

Validation experiments are of great importance for the development of modern computational methods and for the understanding of physical phenomena. In order to ensure comparability between simulation and experiment, the experimental conditions need to be modeled as accurately as possible in the simulation setup. However, the computational effort increases significantly when the full geometric configuration of a wind tunnel experiment is taken into account. Therefore, simplifications of the setup in combination with correction factors are often used to mimic wind tunnel effects. In the context of aircraft computational fluid dynamics (CFD), it is desirable to handle the isolated aircraft geometry without the added complexity of the surrounding wind tunnel structure.

The physical effects of a mounting system on the flow around the model can be divided in a near-field and far-field effect, as Stojanowski et al. [13] point out. Similarly, Britcher et al. [1] describe three components of interference: overall, local and geometrical modification. The overall effect of the sting on the flow is due to the pressure gradient induced by the sting's physical blockage. The local flow disturbance is caused by interference between support system and

A. Dillmann et al. (Eds.): STAB/DGLR Symposium 2020, NNFM 151, pp. 3–13, 2021.
https://doi.org/10.1007/978-3-030-79561-0_1

flow in the vicinity of the model, most significantly by altering the development of boundary layers. Finally, the geometrical distortion results from altered model surfaces such as e.g. the interface between sting and model replacing a fuselage surface or a tailcone.

Prior work dealing with flow separation and the wake of the NASA Common Research Model (CRM) [14] in free flight conditions has been carried out in the authors' working group [15,17]. Waldmann et al. [15] showed the necessity of using hybrid RANS/LES methods for the resolution of the complex flow in the separated wake associated with the behavior of the wing leading edge shear layer in post stall conditions. They concluded that the aerodynamic coefficients and the wake propagation can be predicted in good agreement with the experiment by using the Delayed Detached Eddy Simulation method (DDES) [11]. The experimental data used for comparison was taken from the measurement campaign conducted during the ESWI^{RP} project in the European Transonic Wind Tunnel (ETW) [7].

As the simulations in the previously mentioned publications are based on the free flight configuration of the CRM, wind tunnel effects such as wall interference and mounting system are not taken into account. The wind tunnel wall influence is minimized in ETW by the use of slotted walls, and it has been studied in the context of the ESWI^{RP} campaign [3]. However, the wind tunnel model differs from the free flight configuration in the area of the rear fuselage, which includes the interface with the model support system. This leads to inherent differences between wind tunnel and simulation results, and increases uncertainties.

For this reason, different wind tunnel effects such as the wall influence and the impact of the blockage effect of the model support system have been subject of recent research. The influence of the wind tunnel support system on the CRM's flow characteristics has been characterized in the transonic regime [4,6,8] and in the linear range of the angle of attack polar at subsonic conditions [16]. While these studies quantify the influence of the mounting on the aerodynamic coefficients, the wing pressure distribution, and the local flow at the aircraft's tail, its effect on the post stall flow is still insufficiently explored. This flow regime at the edge of the flight envelope is of particular interest because the occurring unsteady aerodynamic loads can cause damage to the aircraft structure and may lead to controllability issues. The present computational study deals with the question of how the mounting of the wind tunnel model affects the propagation of the wake and its interaction with the horizontal tailplane at subsonic flow conditions and at high angles of attack. Knowledge of these effects provides quantitative data on expected differences involved in comparisons of free flight simulations with wind tunnel data. Therefore, more reliable statements towards the development of the turbulent wake can be made.

2 Test Case and CFD Setup

The present work focuses on simulations of the CRM in the post stall regime with the hybrid RANS/LES model DDES. The computational model geometry

Table 1. Flow conditions and geometric parameters

Ma_∞	Re_∞	p_0	T_0	c_{ref}	α
0.25	$11 \cdot 10^6$	303 kPa	115 K	0.189 m	18°

replicates the wind tunnel model as used in ESWI^{RP} [7]. The flow conditions which reproduce run 316 of that campaign as well as the main geometric parameters of the model are listed in Table 1 where p_0 and T_0 denote the total values of pressure and temperature, c_{ref} is the mean aerodynamic chord and α the angle of attack. The data from the ESWI^{RP} [7] campaign include corrections for the wall interference, flow curvature and Mach effects. This study employs the dataset without sting buoyancy correction in order to better isolate the sting's influence on the flow field around the model.

The TAU solver [9] provided by DLR is used for all simulations in the present work. This finite volume solver is second order accurate in space and time using a central differencing scheme for the convective fluxes and an implicit backward Euler scheme with dual time stepping for time discretization. In order to reduce dissipation of small scale turbulent structures and avoid excessive dissipation of small scale instabilities, low dissipation settings are applied incorporating DLR's recommendations for hybrid RANS/LES simulations [2]. More precisely, a matrix-based artificial dissipation approach with a fourth order dissipation coefficient of $k^{(4)} = 1/1024$ is used. A blending between scalar-valued and matrix-valued dissipation models is set up such that matrix-valued dissipation contributes 95% of the total. Furthermore, the mean flow fluxes are discretized using the skew-symmetric scheme by Kok [5]. The dual time stepping scheme employs a physical time step size corresponding to 1% of the convective time unit $t_\infty = c_{\text{ref}}/u_\infty$. This yields a time step of $\Delta t = 3.461 \cdot 10^{-5}$ s. The mean and fluctuating values investigated in this work are obtained from time series spanning $70t_\infty$, which were extracted from longer simulated time series ensuring that no transient effects associated with simulation start-up remain in the solution.

The two investigated configurations represent the CRM with a horizontal tailplane, which is mounted at an incidence of 0° with respect to the fuselage (WBT0 configuration). The wing deformation due to aerodynamic loads in the wind tunnel is taken into account by deforming the grids according to the deformation recorded in the measurement campaign. More details about the deformed shapes and the grid deformation process can be found in Lutz et al. [7] and Waldmann et al. [15]. Waldmann et al. [16] quantified the improvement of computational results, which can be achieved by including the wing deformation. This deformation leads to the WBT0d configuration without wind tunnel support system, which is similar to the grid presented in [15]. The configuration WBT0ssd additionally takes into account the CRM's wind tunnel mounting sting which enters the fuselage in place of a vertical tailplane. The arc sector the sting is attached to in the ETW is not included in the computational model. The sting is cut off in the region where it enters the arc sector after its cylindrical part has

reached maximum diameter. The sting's aft end is closed using a hemispherical cap. In the previous investigation of Waldmann et al. [16] this modeled length of the sting was sufficient for capturing the support system's influence on the flow around the CRM. Both configurations are represented in Fig. 1.

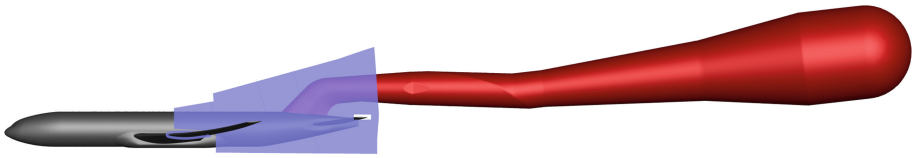

Fig. 1. CRM with and without wind tunnel mounting. Slice through structured wake grid in blue. Sting shown in red.

Two grids created with the CFD mesh generation software Pointwise are used in the present work. They are identical except in the region of the rear fuselage and the sting. The boundary layers are resolved using prism and hexahedron layers, ensuring $y^+ < 1$ everywhere. The area above the wing's suction side and the wake area is discretized using isotropic hexahedral elements in order to ensure a mesh suitable for scale resolving methods in areas of separated flow. A slice through this structured grid area is depicted in blue in Fig. 1. The structured area resolving the separated wake is also identical in both grids.

The junction areas between fuselage and wing, tailplane and wind tunnel mounting system, respectively are meshed using fully structured grid blocks. This enables the resolution of corner flow effects occurring in these areas. Overall, the WBT0d mesh consists of approx. 51 million points, whereas the WBT0ssd grid contains approx. 59 million grid points.

The one-equation Spalart-Allmaras (SA) turbulence model [10] is used as background model for DDES, as in the original model presented by Spalart. SA does not include the f_t and f_{t2} terms in this implementation. All runs are conducted assuming fully turbulent flow due to high Reynolds number and an extreme angle of attack with highly accelerated flow velocities around the leading edge. The hybrid RANS/LES simulations use a filter width based on the maximum edge length of the grid cells. This Δ_{max} filter in combination with the chosen timestep results in a convective CFL number between 1 and 2 in the area of flow separation on the employed grids. Following Spalart's [12] recommendation for DES-type grids, and prior work of Waldmann et al. [15], this is sufficient for resolving the major turbulent scales in the separated wake.

3 Results

The following section comprises studies of local flow effects caused by the support system near the aircraft tail as well as the influence on the wake. In addition to overall lift, drag and pitching moment data, the alteration of the local flow angle in the wake and its impact on the tailplane inflow are quantified and analyzed.

3.1 Near Field Effects

The sting's presence alters the local flow field in its immediate vicinity and forces the incoming flow to move around it instead of remaining largely straight above the fuselage. Figure 2 shows the pressure distribution and surface streamlines in the rear fuselage region of the CRM and on the upstream part of the wind tunnel mounting. The sting forces the flow outward in the spanwise direction. This displacement effect leads to a downward deflection of the surface streamlines upstream of the horizontal tailplane. The flow is locally accelerated around the sting, resulting in the low surface pressure region around the widest area of the vertical portion. Near the tailplane leading edge root and above the upper side of the tailplane, an upward bend and a stronger curvature of the surface streamlines can be observed in the presence of the sting.

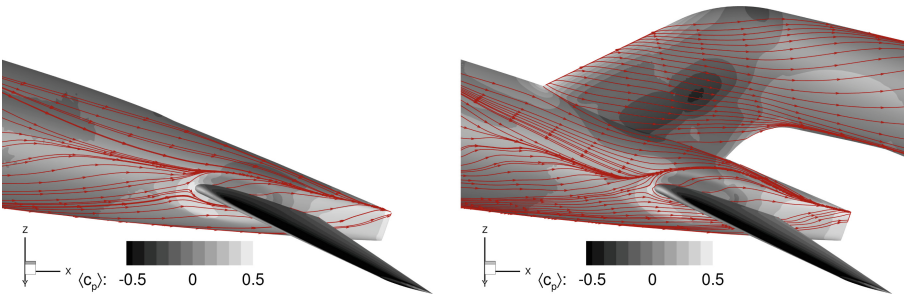

(a) WBT0d configuration (b) WBT0ssd configuration

Fig. 2. c_p and surface streamlines at the rear fuselage of the CRM and the sting.

The difference of the surface pressure coefficient Δc_p on the fuselage caused by the support system is shown in Fig. 3. An increase in local pressure, both upstream and downstream of the area where the sting enters the fuselage is clearly visible. This can be attributed to decelerated flow in these areas. Furthermore, Δc_p on the fuselage's surface is reduced in the region of accelerated flow near the widest point of the sting. The positions of these regions are in agreement with those of Waldmann et al. [16] at lower angles of attack but show a slightly larger magnitude. In addition, the pressure coefficient is increased near the leading edge of the horizontal tailplane when the support system is included. This is due to the reduction of the local flow field angle upstream of the tailplane, which is considered further below.

Figures 4 and 5 visualize the difference of the local flow field angle ξ between the cases with and without the wind tunnel support system. A plane at $\eta = 10.7\%$ of wing semi-span $\eta = y/b$ and a plane upstream of the tailplane and parallel to its leading edge are examined, respectively. The angle ξ is defined with respect to the horizontal inflow direction, i.e. $\xi = \arctan(w/u)$. Generally, Fig. 4 implies that the deflection is directed upward above the sting and downward

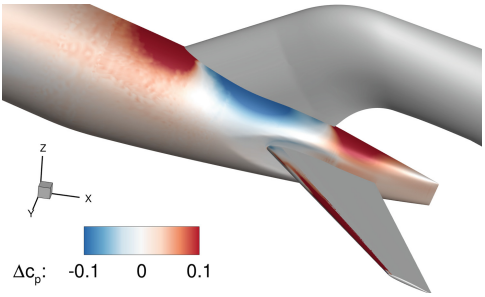

Fig. 3. Pressure difference due to the support system, $\Delta c_p = c_{p,WBT0ssd} - c_{p,WBt0d}$.

below it. This is also indicated by the surface streamlines on the horizontal sting portion in Fig. 2 b). More precisely, the flow displacement due to the sting volume decreases the local flow angle below the sting's spanwise widest point, which includes the flow volume interacting with the tailplane. In the same manner, the flow above the widest point is deflected upwards. ξ is decreased by approximately 2° upstream of the tailplane leading edge in the section shown in Fig. 4. This tendency can be observed over the entire half span in Fig. 5. Except in a small region of positive $\Delta\xi$ at approximately 25% of the halfspan, the tailplane encounters a decrease of the inflow angle. The strongest downward deflection of the flow can be observed near the fuselage surface and, with increasing absolute value, toward the tailplane tip. In the tip region, ξ is decreased by approximately 2° in a large area above the tailplane. From this follows a decrease in the local angle of attack throughout the tailplane halfspan and thus a lower lift coefficient. The flow over the tailplane is attached in both cases except for a small separation bubble near the leading edge in the tip region. This small separation has no significant impact on the tailplane loads. These loads as well as the overall lift and the airplane's pitching moment are examined in Sect. 3.3.

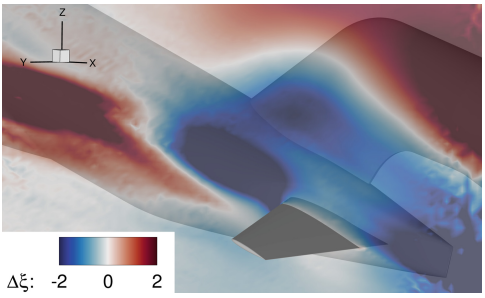

Fig. 4. Increment of the local flow field angle $\Delta\xi = \xi_{WBT0ssd} - \xi_{WBTd}$ at $\eta = 10.7\%$.

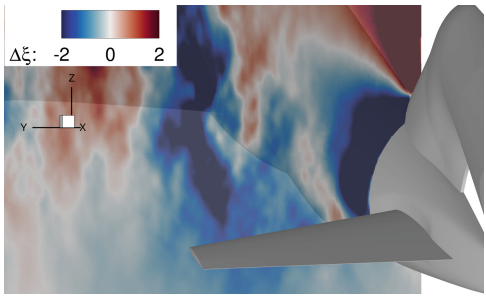

Fig. 5. Increment of the local flow field angle $\Delta\xi = \xi_{WBT0ssd} - \xi_{WBT0d}$ parallel to the htp leading edge.

3.2 Far Field Effects

Figure 6 compares the wake sizes of the two configurations using isolines of the mean streamwise velocity $u/u_\infty = 0.9$. Three planes of constant x/c_{ref} are considered, starting near the trailing edge at $x/c_{ref} = 6$ up to $x/c_{ref} = 9$. The location of these slices is indicated in the bottom center of Fig. 6. The wake extent at $x/c_{\text{ref}} = 6$ in the vicinity of the inboard wing trailing edge shows only minor differences between the two configurations. When progressing to the two downstream planes, the influence of the sting shifts the upper edge of the wake upwards for spanwise positions between $\eta = 0$ and 0.2. In the middle streamwise slice at $x/c_{\text{ref}} = 7.5$, the lower edge of the wake is shifted downwards in the WBT0ssd configuration. This effect is visible up to a spanwise coordinate of $\eta = 0.45$. The most downstream wake plane at $x/c_{\text{ref}} = 9$ shows an increased downward shift of the lower limit of the wake from $\eta = 0$ to $\eta = 0.45$ in comparison to the medium wake position. Further outboard the differences in the wake diminish in all regarded planes. This trend of increasing wake size, especially by shifting the lower wake boundary, is in agreement with the aforementioned far field influence of the sting. While the upper wake edge shows no displacement of the wake except near the sting, the downward deflection of the flow by the wind tunnel support system affects the lower wake edge, which is shifted downwards as the downstream position increases. Effectively, the sting's presence slightly slows down the flow in front of it, thereby widening the wake. The sting's location shifts the overall wake slightly downward. This effect vanishes upstream toward the wing and with increasing spanwise position, i.e. the far field effect is of rather limited spatial extent. Consequently, no such effect can be detected in the vicinity of the wing. The flow separation on the wing and its lift therefore do not show any major influence from the support system.

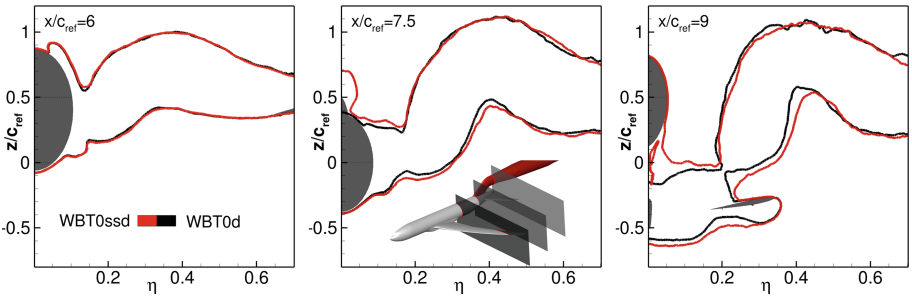

Fig. 6. Wake extent in streamwise planes at $x/c_{\mathrm{ref}} = 6, 7.5, 9$ with lines of $\overline{u}/u_\infty = 0.9$. Fuselage, wing, tailplane and sting in grey.

3.3 Forces and Moments

The local downward deflection caused by the sting in the tailplane's vicinity is associated with decreased lift, as a consequence of the decreased angle of attack of the tailplane. The distributions of C_L over the tailplane span are shown in Fig. 7. The absolute difference between the two cases increases towards the horizontal tailplane's tip. At the same time, the variance of the tailplane lift is consistently higher in the presence of the sting. This results from the downward deflection of the turbulent wake depicted in Fig. 5. As a result, more of the incoming turbulent structures flow toward the tailplane and impinge load. Even though the mean load is decreased by the sting, the fluctuations and therefore the dynamic tailplane loads grow. This is consistent with the observation that load fluctuations are not due to flow separation on the tailplane, but result exclusively from inflow turbulence.

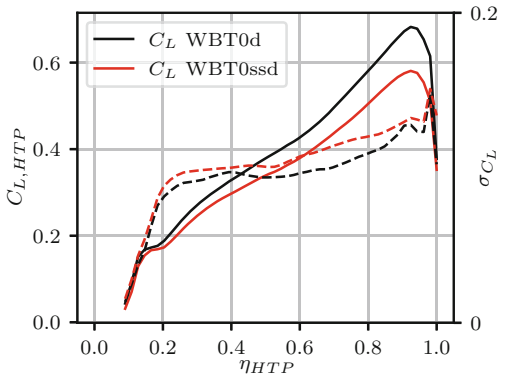

Fig. 7. Spanwise distributions of lift coefficient $c_l(\eta)$ on the horizontal tailplane. Dashed lines denote the variance, corresponding to the right-hand axis.

Time-averaged forces and moments of the two configurations under consideration as well as the experimental values are shown in Table 2. The experimental data does not include forces separated into wing and tailplane contributions, and the total aircraft lift coefficients differ only little. While the WBT0d configuration overpredicts the overall lift C_L, it is underpredicted by the WBT0ssd configuration. The differences in $C_{L,wing}$ are of a comparably small magnitude. The more pronounced difference in $C_{L,HTP}$ cannot be evaluated in terms of accuracy due to lack of experimental data, it is however possible to use the pitching moment C_{My} in its stead. While the WBT0d configuration overpredicts the nose down pitching moment C_{My} by 25%, the WBT0ssd underpredicts it by about 16%. This indicates that slightly better agreement with the experimental values of the pitching moment can be achieved when considering the wind tunnel support system. However, it also indicates that the pitching moment is sensitive to the CFD modeling setup. The drag coefficient C_D decreases slightly when the support system is present, which can be attributed to the decreased lift forces acting on both the wing and the tailplane.

Table 2. Time-averaged forces and moments at $\alpha = 18^\circ$ with and without sting.

	C_L	$C_{L,wing}$	$C_{L,HTP}$	C_D	C_{My}
Experiment	1.078	n/a	n/a	0.3276	−0.159
WBT0d	1.09	0.785	0.321	0.336	−0.199
WBT0ssd	1.07	0.775	0.286	0.331	−0.132

4 Conclusions

The above results and discussion showcase and quantify the influence of the wind tunnel support system on the wake of the CRM in post stall at $\alpha = 18^\circ$. In order to evaluate possible errors when neglecting the wind tunnel mounting in numerical simulations, its effect on the surface pressure coefficient, on the flow in the vicinity of the tailplane and on the entire separated wake emanating from the wing were investigated. Furthermore, the effect of the support system on the forces and moments acting at the airplane as well as the comparison to wind tunnel data is part of this investigation.

The impact in the near field of the wind tunnel support system is due to the displacement effect of the sting which reduces the angle of inflow in the entire tailplane region and alters the pressure distribution on the fuselage surface. This near field effect leads to a decrease in tailplane lift over the entire span. A far field effect of the sting upstream toward the wing cannot be observed as the wake size in the wing region and the wing's lift remains largely unchanged when comparing both configurations. Further downstream, the lower edge of the wake is shifted downwards due to the model mounting, the overall wake extent in vertical direction is increased. This brings about an increase of the

tailplane's lift fluctuations due to stronger impingement of the propagated wake turbulence onto its surface. In terms of the overall forces and moments, taking into account the wind tunnel support system leads to a slightly better accordance of all values with the experiment. The overall lift shows a slight decrease when considering the wind tunnel support system, which also leads to a decrease of the overall drag. Furthermore, the decrease of the tailplane lift leads to a lower nose down pitching moment. These small improvements come at the expense of the meshing effort and increase the simulation time due to the rising number of grid points. However, if the flow field near the aircraft's tail is to be investigated, a consideration of the wind tunnel mounting system is recommended because of the sting's deflection of the flow in this area of the wake. A more detailed study on the changing interaction of wake turbulence with the tailplane boundary layer is part of future research.

Acknowledgements. The authors gratefully acknowledge the Deutsche Forschungsgemeinschaft DFG (German Research Foundation) for funding this research in the project LU 809/8. Furthermore, we would like to thank DLR for providing the TAU source code. The computational resources for the simulations were kindly provided by the High Performance Computing Center Stuttgart (HLRS).

References

1. Britcher, C.P., Alcorn, C.W., Kilgore, W.A.: Subsonic sting interference on the drag of a family of slanted-base ogive-cylinders, AIAA 89-2006-CP (1989)
2. Deutsches Zentrum für Luft- und Raumfahrt. DLR TAU-code user guide (2018)
3. Gorbushin, A., et al.: Slotted wall interference investigation in ETW using the NASA CRM model. AIAA 2015-0621 (2015)
4. Kohzai, M., Ueno, M., Koga, S., Sudani, N.: Wall and support interference corrections of NASA common research model wind tunnel tests in JAXA. AIAA 2013-0963 (2013)
5. Kok, J.C.: A high-order low-dispersion symmetry-preserving finite-volume method for compressible flow on curvilinear grids. J. Comput. Phys. **228**(18), 6811–6832 (2009)
6. König, B., Fares, E.: Validation of a transonic Lattice-Boltzmann method on the NASA common research model. In: 54th AIAA Aerospace Sciences Meeting, San Diego, California, USA, AIAA 2016-2023, January 2016
7. Lutz, T., Gansel, P.P., Waldmann, A., Zimmermann, D.-M., Schulte am Hülse, S.A.: Time-resolved prediction and measurement of the wake past the CRM at high reynolds number stall conditions. J. Aircraft **53**(2), 501–514 (2016)
8. Rivers, M., Hunter, C., Campbell, R.: Further investigation of the support system effects and wing twist on the NASA common research model. AIAA 2012-3209 (2012)
9. Schwamborn, D., Gerhold, T., Heinrich, R.: The DLR TAU-Code, recent applications in research and industry. In: European Conference on Computational Fluid Dynamics ECCOMAS CFD 2006, September 2006
10. Spalart, P.R., Allmaras, S.R.: A one-equation turbulence model for aerodynamic flows. Recherche Aerospatiale **1**, 5–21 (1994)

11. Spalart, P.R., Deck, S., Shur, M.L., Squires, K.D., Strelets, M., Travin, A.: A new version of detached-eddy simulation, resistant to ambiguous grid densities. Theoret. comput. Fluid Dyn. **20**(3), 181 (2006)
12. Spalart, P.R., Streett, C.: Young-person's guide to detached-eddy simulation grids. Technical report, NASA CR-2001-211032 (2001)
13. Stojanowski, M., Germain, E.: The falcon 7x from ETW to flight. AIAA 2008-835 (2008)
14. Vassberg, J.C., DeHaan, M.A., Rivers, M.B., Wahls, R.A.: Development of a common research model for applied CFD validation studies. In: 26th AIAA Applied Aerodynamics Conference, August 2008
15. Waldmann, A., Gansel, P.P., Lutz, T., Krämer, E.: Unsteady wake of the NASA common research model in low-speed stall. J. Aircraft **53**(4), 1073–1086 (2016)
16. Waldmann, A., Lutz, T., Krämer, E.: Wind tunnel support system influence on NASA common research model at low speed condition. J. Aircraft **55**(5), 1762–1772 (2018)
17. Zimmermann, D.-M., Waldmann, A., Lutz, T., Krämer, E.: Development of flow structures in the near-field wake region of the common research model. CEAS Aeronautical J. (2016)

Assessment of the Disturbance Velocity Approach to Determine the Gust Impact on Airfoils in Transonic Flow

Jens Müller(✉), Marco Hillebrand, and Thorsten Lutz

Faculty 6: Aerospace Engineering and Geodesy, Institute of Aerodynamics and Gas Dynamics, University of Stuttgart, Pfaffenwaldring 21, 70569 Stuttgart, Germany
jens.mueller@iag.uni-stuttgart.de

Abstract. Unsteady CFD simulations of vertical "1-cos" gusts interacting with the DLR-F15 airfoil at transonic flow conditions are analyzed. The scope of the work is to assess the applicability of the simplified Disturbance Velocity Approach (DVA) for gust simulation, which is implemented in the CFD code TAU. While the DVA covers the interaction of the gust with the airfoil, it neglects the effect of the airfoil and the flow around the airfoil on the gust. Simulations where the gust and all interactions are resolved within the flow field are used to evaluate the accuracy of the DVA. Gust wavelength and angle of attack are varied to ensure a reliable assessment of the DVA. Lift, pitching moment, and shock position can be accurately determined by the DVA. At higher angles of attack and a small gust wavelength, the DVA's drag history shows deviations which should be taken into account. Overall, the DVA provides suitable results with respect to the resolved gust simulations.

Keywords: Aircraft aerodynamics · CFD · Gust loads

1 Introduction

In cruise flight aircraft encounter atmospheric disturbances like gusts which directly affect passenger comfort and structural loads. In order to diminish the negative impact of gusts on the aircraft, the development of gust load alleviation concepts becomes important. This requires accurate and industrially applicable simulation methods to determine the effect of atmospheric gusts on aircraft aerodynamics and structural loads. The accuracy of methods based on potential flow theory, like the unsteady vortex lattice or the doublet-lattice method (DLM) is limited, especially in cruise flight, since they neglect transonic and viscous effects [1]. A transonic correction can be applied to the DLM using specific weighting factors or results based on wind tunnel tests or CFD simulations [2]. Complete coverage of the effects mentioned above is possible when utilizing CFD, which makes it a suitable approach for the analysis of gust interaction. The highest accuracy when simulating gust interaction with CFD is achieved when the gust is resolved and propagated within the flow field. This method is called the

A. Dillmann et al. (Eds.): STAB/DGLR Symposium 2020, NNFM 151, pp. 14–23, 2021.
https://doi.org/10.1007/978-3-030-79561-0_2

Resolved Atmosphere Approach (RAA) [3]. It covers both the impact of the gust on the aircraft as well as the impact of the aircraft on the gust [4]. The main drawback of this method is the high computational effort due to the fine mesh resolution needed to reduce numerical dissipation and dispersion effects during the propagation of the gust. This limits the industrial application. Therefore, simplified methods for gust interaction simulation in CFD like the split velocity method [5] or the Disturbance Velocity Approach (DVA) [4] were developed where the latter is used within this work. The DVA enables the usage of standard CFD grids without any special refinement, but covers only the influence of the gust on the aircraft. Different to the RAA, the effect of the aircraft on the gust is neglected within the DVA. Hence, the question arises to what extend the DVA is applicable for gust interaction simulation.

Both RAA and DVA were implemented into the flow solver TAU [6] by Heinrich and Reimer [4]. They provide a first assessment of the accuracy of the DVA compared to the RAA by analyzing the lift history of two consecutive NACA 0012 airfoils and an aircraft configuration encountering vertical "1-cos" gusts of different wavelengths at sub- and transonic speeds [3,4]. For subsonic flow conditions these investigations were extended in [7] where vertical "1-cos" gusts interact with a single airfoil. Gust wavelength, angle of attack, and airfoil shape were varied. These studies show that for gust wavelengths larger than the chord length the DVA provides suitable results. At subsonic speeds the pitching moment turned out to be the most critical parameter regarding the accuracy of the DVA. The DVA is also applicable to airfoils or wings interacting with broadband atmospheric turbulence at subsonic speeds, as shown in [8,9]. The scope of the work at hand is to extend the investigations in [3,4,7] to a detailed assessment of the applicability of the DVA to supercritical airfoils at transonic speeds. Compared to the NACA 0012 airfoil investigated in [4], the DLR-F15 airfoil [10] used within this work is representative of supercritical airfoils designed for transonic flow conditions. The utilization of an airfoil compared to a full aircraft configuration enables the assessment of specific effects occurring at a wing section which influence the accuracy of the DVA. Lift, drag, and pitching moment history resulting from CFD simulations of the DLR-F15 airfoil encountering a vertical "1-cos" gust are evaluated. For different gust wavelengths and angles of attack the results of the DVA are compared to the RAA results in order to assess the applicability of the DVA.

2 Numerical Methods and Setup

The numerical approach, as well as mesh generation, follows Müller et al. [7]. Further details can be found there. The finite volume Navier-Stokes solver TAU [6] is applied for the CFD simulations within this work. The solver developed by the German Aerospace Center (DLR) provides a second order accuracy in time and space. In order to represent atmospheric gusts in CFD simulation the Resolved Atmosphere Approach and the Disturbance Velocity Approach are used. A detailed description of RAA and DVA can be found in [3,4]. The RAA represents the physically accurate reference for gust interaction simulation in CFD.

Here, modified unsteady far field boundary conditions are used to feed the gust into the flow field. At these boundary conditions the far field velocity at each cell is dependent on time and space, with the disturbance velocities $\mathbf{u}'$ of the gust added to the mean velocity of the flow [4]. After being fed into the flow field the gust is fully resolved and propagated within the flow field.

Within the DVA the time dependent disturbance velocities $\mathbf{u}'$ are treated similar to grid velocities. At each cell $\mathbf{u}'$ is added to the flux balance by superposition. With the convection across the cell interfaces changed from $\mathbf{u} - \mathbf{u}_b$ to $\mathbf{u} - \mathbf{u}_b - \mathbf{u}'$, where $\mathbf{u}_b$ is the velocity of the boundary of a control volume [4], the continuity equation changes to

$$\frac{d}{dt} \int\limits_V \rho \, dV + \oint\limits_S \rho(\mathbf{u} - \mathbf{u}_b - \mathbf{u}') \cdot \mathbf{n} \, dS = 0. \tag{1}$$

Within this work the supercritical DLR-F15 airfoil [10] interacting with a vertical "1-cos" gust is evaluated. The flow conditions correspond to transonic cruise flight at 35,000 feet with Mach number $M = 0.74$, angle of attack $\alpha = 1.1°$, and Reynolds number $Re = 20.2 \cdot 10^6$ with respect to the chord length c of the airfoil. The amplitude of the vertical "1-cos" gust is set to $A_{gust} = 10\text{m/s}$. The resulting vertical gust velocity w, as a function of the gust wavelength λ, is defined according to the EASA certification specification CS 25.341 as

$$w(x) = \frac{A_{gust}}{2} \left[1 - \cos\left(\frac{2\pi x}{\lambda} \right) \right] \quad \text{with} \quad 0 \leq x \leq \lambda. \tag{2}$$

In order to evaluate the accuracy of the DVA at transonic cruise flight conditions two parameters are varied within this work. First, the gust wavelength λ is varied at a constant angle of attack of $\alpha = 1.1°$. λ is set to $\lambda = c$, $\lambda = 2c$, and $\lambda = 4c$. Second, the angle of attack is changed to $\alpha = 0°$ and $\alpha = 2.2°$ with a constant gust wavelength $\lambda = c$. At all cases unsteady RANS simulations are performed. The Spalart-Allmaras turbulence model is applied. Within the dual time-stepping approach of TAU, 250 inner iterations per time step are used with a physical time step size of $\Delta t / t_{ref} = 0.005$. The reference time $t_{ref} = c/u_\infty$ is the time a gust needs to travel a distance of one chord length. u_∞ denotes the freestream velocity. Similarly to [7], the Chimera overset grid method is used to represent different angles of attack within the RAA and DVA simulations. This results in a background grid and a separate airfoil grid. The airfoil grid is fully structured and identical for both RAA and DVA simulation in order to avoid any numerical differences. Due to the transonic flow regime a shock is present on the upper side of the airfoil. To ensure the correct resolution of the shock the number of points on the airfoil surface is increased in this region. The chordwise position of the refined shock region is adapted to the local shock position for each individual angle of attack. It is also ensured that the shift in the shock position due to the gust interaction is covered by the refined region. The boundary layer is resolved and $y^+ < 1$ is ensured.